THE JOURNAL OF PHYSICAL CHEMISTRY C

Article

pubs.acs.org/JPCC

Thermal and Optical Characterization of Undoped and Neodymium-Doped $Y_3ScAl_4O_{12}$ Ceramics

Maria Cinta Pujol,*[,†] Alexandre Maitre,[‡] Julie Carreaud,[‡] Rémy Boulesteix,[‡] Alain Brenier,[§] Guillaume Alombert-Goget,[§] Yannick Guyot,[§] Joan Josep Carvajal,[†] Rosa Maria Solé,[†] Jaume Massons,[†] Alberto Oleaga,[∥] Agustín Salazar,[∥] Isabel Gallardo,[⊥] Pablo Moreno,[#] Javier Rodríguez Vázquez de Aldana,[#] Magdalena Aguiló,[†] and Francesc Diaz[†]

[†]Física i Cristal·lografia de Materials i nanomaterials (FiCMA-FiCNA)-EMAS, Universitat Rovira i Virgili, Campus Sescelades, c/Marcel·lí Domingo, s/n, 43007 Tarragona, Spain

[‡]Laboratoire Science des Procédés Céramiques et Traitements de Surface, UMR CNRS 7315, Université de Limoges, 87068 Limoges, France

[§]Institut Lumière Matière, UMR5306 Université Lyon 1-CNRS, Université de Lyon, 69622 Villeurbanne Cedex, France

[∥]Departamento de Física Aplicada I, Escuela Técnica Superior de Ingeniería, Universidad del País Vasco, UPV/EHU, Alameda Urquijo s/n, 48013 Bilbao, Spain

[⊥]Centro de Láseres Pulsados (CLPU), C/Adaja s/n, 37185 Villamayor, Salamanca, Spain

[#]Grupo de Investigación en Microprocesado de Materiales con Láser, Universidad de Salamanca, Plaza de la Merced s/n, 37008 Salamanca, Spain

ABSTRACT: $Y_{3-3x}Nd_{3x}Sc_1Al_4O_{12}$ (x = 0, 0.01, and 0.02) ceramics were fabricated by sintering at high temperature under vacuum. Unit cell parameter refinement and chemical analysis have been performed. The morphological characterization shows micrograins with no visible defects. The thermal analysis of these ceramics is presented, by measuring the specific heat in the temperature range from 300 to 500 K. Their values at room temperature are in the range 0.81−0.90 J $g^{-1}K^{-1}$. The thermal conductivity has been determined by two methods: by the experimental measurement of the thermal diffusivity by the photopyroelectric method, and by spectroscopy, evaluating the thermal load. The thermal conductivities are in the range 9.7−6.5 W K^{-1} m^{-1} in the temperature interval from 300 to 500 K. The thermooptic coefficients were measured at 632 nm by the dark mode method using a prism coupler, and the obtained values are in the range 12.8−13.3 × 10^{-6} K^{-1}. The nonlinear refractive index values at 795 nm have been evaluated to calibrate the nonlinear optical response of these materials.

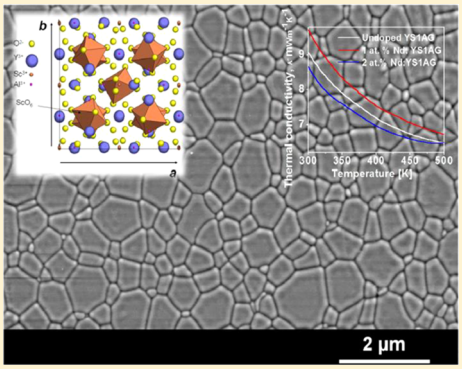

1. INTRODUCTION

New ceramic materials belonging to the family of garnet compounds are emerging as a promising alternative for high power lasers. Among them, $Y_{3-3x}Nd_{3x}Sc_1Al_4O_{12}$ (x = 0.01 and 0.02, hereafter 1 and 2 atom % Nd:YS1AG) presents interesting features such as the long lifetime of Nd^{3+} emitting levels and the broad line widths due to its disordered structure (Sc^{3+} is randomly found in the positions of Al^{3+}). Replacing Al^{3+} ions with larger Sc^{3+} ions increase the distance between dodecahedral lattice sites (substitutional sites for Nd^{3+}) and tend to reduce the relatively strong Nd^{3+} ion−ion interaction encountered in YAG associated with the concentration quenching of Nd^{3+} fluorescence.[1] In addition, Ober et al. generated 260 fs pulses using Nd^{3+}-doped mixed scandium garnets like Nd:YS1AG.[2] The disordered nature of these crystals induces a strongly inhomogeneous broadening of both fluorescence and absorption bands, which is favorable for obtaining pulsed laser operation.

Recently, the evolution of the fluorescence of Nd^{3+} with temperature in the YS1AG matrix has been studied;[3,4] it was demonstrated that the temperature of the gain medium has a strong effect upon the fluorescence spectrum and the laser properties of the YS1AG ceramic. In particular, these works have shown that depending on the temperature, a Nd:YS1AG ceramic laser can operate selectively at 1061 or 1064 nm, or simultaneously at both wavelengths with a strong gain structuration.

Another interesting advantage is that ceramic materials might have a lower manufacturing cost than traditional bulk crystal

Received: March 19, 2014
Revised: June 3, 2014
Published: June 4, 2014

   dx.doi.org/10.1021/jp5027493 | J. Phys. Chem. C 2014, 118, 13781−13789

since the sintering temperature is significantly lower than their melting point, the temperature needed to be reached for growth of these materials. Additionally, it is known that the ion doping levels can be larger in ceramics than in single crystals and that ceramic processing allows manufacturing of multiple shapes and designs.[5] The fabrication of laser materials with a disordered nature leads to avoiding the imperfection due to different segregation processes and makes the uniformity of the material composition over the whole medium easier.[6]

For high-power laser applications in which the thermal effects such as heat load and thermal lensing are important, the determination of the thermal properties of the amplifier medium is crucial. In particular, the thermal conductivity is an important parameter for a laser active material because it indicates how easily heat wastes can be dissipated, and it determines the maximum pumping density that a material can sustain without excessive optical distortion and stress. Among the different lanthanide hosts, the thermal conductivity of the garnet family is one of the largest. Additionally, the knowledge of the thermooptical coefficient, which governs the thermal lensing effects, can help in controlling it.

The nonlinear refractive index coefficient, n_2, is related to the self-focusing effect as well as to the nonlinear absorption coefficient present in the gain medium at high pumping levels, so knowledge of this parameter is important for high-power laser applications.

In ceramics, some defects generally encountered such as secondary phases, pores, or grain boundaries could affect the heat diffusion. It is known that at room temperature, the thermal conductivity, κ, is not affected by the existence of grain boundaries since the intrinsic thermal resistance due to interaction between phonons dominates. On the other hand, at low temperature, the phonon−phonon interaction is strongly reduced; leading to only extrinsic contributions from defects, including grain boundaries. Thus, the polycrystalline material displays a lower thermal conductivity by about 1 order of magnitude. All this suggests that specific defects in ceramics contribute to reduce the thermal conductivity at low temperatures.[7]

The nonlinear refractive index, n_2, is another important point to be considered in the design of high-power solid-state lasers and related optical systems. In the case of a medium with a high nonlinearity, the self-action of a powerful laser beam involves the effects of self-focusing and self-phase modulation. In general, the measured values of n_2 in ceramic samples are rather close to those corresponding to single crystals and tend to increase if the linear refractive indices of the materials increase. This tendency is well-known and confirmed for many media.[8]

The present work is devoted to characterize the thermal and optical properties of a new family of ceramic materials, the YS1AG. A detailed study of these properties allows a better understanding of the behavior of this ceramic material during high power laser action operation.

2. EXPERIMENTAL DETAILS

Description of the Ceramic Synthesis Method. The ceramic samples were elaborated according to a process detailed elsewhere.[9] In short, submicrometer α-Al_2O_3 (purity >99.99%, Baïkowski, France) Y_2O_3 (purity >99.99%, Alfa Aesar, Germany), Sc_2O_3 (purity >99.9%, Auer Remy, Germany), and Nd_2O_3 (purity >99.99%, Alfa Aesar, Germany) powders were mixed together in stoichiometric proportions to form after thermal treatment the $Y_{3-3x}Nd_{3x}Sc_1Al_4O_{12}$ (x = 0, 0.01 and 0.02) garnet phase. Powder mixing was carried out by using ball milling in water with different amounts of SiO_2 (up to 0.3 wt %) as sintering aid. After drying and applying cold uniaxial press, the green pellets produced were heated at temperatures higher than 1173 K in air atmosphere to remove organic residues. Sintering was conducted in a tungsten mesh-heated furnace under vacuum ($P \leq 10^{-2}$ Pa) at a temperature of 2023 K for 10 h. The specimens were placed in an alumina crucible, and heating and cooling rates of 5 K min^{-1} were applied.

Composition and Structural Characterization. The chemical composition of the samples was measured by electron probe microanalysis. The samples were embedded in an epoxy resin, and polished to perform the surface analysis. The X-ray lines and standards used were Lα and YAG, Kα and Sc, Kα and Al_2O_3, and Lα and REE4 for Y, Sc, Al, and Nd concentration determination, respectively. With the experimental parameters used, the Nd detection limit was 0.033 in weight %, and, in all cases, the neodymium concentration obtained was above this detection limit, ensuring a correct determination of the concentration.

X-ray diffraction (XRD) measurements were made using a Siemens D5000 diffractometer (Bragg−Brentano parafocusing geometry and vertical θ−θ goniometer) fitted with a curved graphite diffracted-beam monochromator, diffracted -beam Soller slits, a 0.06° receiving slit, and a scintillation counter as detector. The angular 2θ diffraction range was between 104° and 111°. The data were collected with an angular step of 0.02° at 16 s per step and sample rotation. Cu Kα radiation was obtained from a copper X-ray tube operated at 40 kV and 30 mA. The surface of the sample was dusted with Si (SRM 640b) as the standard. The X-ray diffractogram was analyzed using the Fundamental Parameters Approach convolution algorithm[10] implemented in the program TOPAS.[11] The refined parameters included the unit cell parameter, the 2θ zero error, the background coefficients, the integrated peak intensities, and the full width at half-maximum of a Lorentzian profile to describe the peak broadening induced by the crystallite size.

Before microstructural observation, the sintered samples were polished and thermally etched at 1923 K under air during 1 h in order to reveal their grain structure. Microstructural observations were carried out by using conventional scanning electron microscopy (SEM; Philips XL30).

Thermal Parameters Measurement Techniques. The heat capacity, C_p, of undoped and Nd-doped YS1AG was measured with a Discovery DSC calorimeter from TA Instruments. The measurements were made using Tzero aluminum pans and a nitrogen flow of 50 cm^3 min^{-1}. The sample mass used in these measurements for the different ceramic compositions was around 4 mg. The calibration of the equipment for C_p measurements was carried out by heating sapphire in vacuum and the cell constant and temperature deviation were calculated with In. The heating ramp used both in the calibration process and in the heat capacity measurements was 10 K min^{-1} and several runs for every calibration step were made to average it. After different heating curves with sapphire, the equipment software averaged and calculated the calibration constant K_{Cp} as a function of the temperature taking into account the theoretical values of the heat capacity of sapphire. The measurements were made from 300 to 500 K, and after several runs were carried out to study the reproducibility, the heat capacity of the different ceramic samples was obtained as a function of temperature. The software of the calorimeter directly gave us the heat capacity of

dx.doi.org/10.1021/jp5027493 | J. Phys. Chem. C 2014, 118, 13781−13789

the samples taking into account the calibration constants of the equipment measured previously.

Thermal diffusivity, D, has been measured using a photopyroelectric setup in the standard back configuration.[12] In this method, the front surface of the sample is illuminated by a modulated light beam, while its rear surface is in contact with a pyroelectric detector, which produces an electrical current proportional to the sample temperature. It has been demonstrated that, when the sample and the sensor are thermally thick (the thickness of the sample, l, is greater than the thermal diffusion length $\mu = (D/\pi f)^{1/2}$); both the phase, ψ, and the natural logarithm of the amplitude of the photopyroelectric current have a linear dependence on the square root of the modulated frequency, $\sqrt{f}$, with the same slope, p. From this slope, the thermal diffusivity of the sample in the direction perpendicular to the surface (the through-thickness thermal diffusivity) can be obtained:[13]

$$D = \frac{\pi l^2}{p^2} \tag{1}$$

First the thermal diffusivity was measured at a reference temperature, $D_{\mathrm{ref}}(T_{\mathrm{ref}})$, followed by a continuous change of the temperature recorded at a fixed frequency at the same time that the phase of the photopyroelectric signal. In fact, the phase changes are directly related to changes in the thermal diffusivity of the sample, in such a way that the temperature dependence of D follows the expression[14]

$$D(T) = \left(\frac{1}{\sqrt{D_{\mathrm{ref}}}} - \frac{\Delta(T)}{l\sqrt{\pi f}} \right)^{-2} \tag{2}$$

where $\Delta(T) = \Psi(T) - \Psi(T_{\mathrm{ref}})$ is the change in a phase for a given change in temperature. It is worth mentioning that this method provides high-resolution measurements since small temperature gradients in the sample produce a good signal-to-noise ratio.

In our experimental setup, a diode laser (λ = 656 nm) with a power of 50 mW is used as the heating source. Its intensity is modulated by a periodic current governed by the computer and serving as the lock-in reference. The pyroelectric transducer is a 350 μm-thick $LiTaO_3$ crystal with Ni−Cr electrodes plated on both surfaces. The samples are attached to the pyroelectric transducer by using an extremely thin layer of highly heat-conductive silicone grease (Dow Corning, 340 Heat Sink Compound). The photopyroelectric current is processed by a two-phase lock-in amplifier, which provides us with a vector signal output comprising the amplitude and phase angle of the signal with respect to those of the reference. Both, sample and detector are placed inside a nitrogen bath cryostat that allows measurements in the temperature range from 77 to 500 K. The accuracy of our diffusivity measurements is estimated to be ±3%.

Plates of undoped YS1AG, together with 1 atom % and 2 atom % Nd:YS1AG have been measured. Their thicknesses are about 0.73 mm. Since these samples are transparent to the diode laser wavelength, the front surface was coated with a very thin graphite layer (≈ 3 μm). Several heating runs from 300 to 500 K at a rate of 0.10 K min^{-1} have been performed. A modulation frequency of 11.0 Hz, high enough to ensure the sample is thermally thick but low enough to guarantee a good signal-to-noise ratio, was used.

In the fractional thermal loading study, the fraction of absorbed pump power converted to heat, as explained in Figure 1, was measured from two methods: a thermal one and a

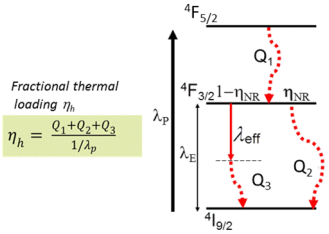

Figure 1. Radiative and nonradiative deexcitation processes in Nd:YS1AG.

spectroscopic one. In the thermal method, the temperature of the sample and its time evolution were recorded with a Pyroview 380L thermal camera (384 × 288 pixels) from Dias Infrared Systems. The calibration of the camera temperature was obtained from a comparison with the temperature measured with a platinum sensor and applying the Stephan law,[15] leading to the emissivity of the studied material.

The sample with mass m was heated with the pump beam from a LIMO fiber coupled laser diode, near 808 nm wavelength. The powers of the incident beam, the reflected beam by the sample, and the transmitted beam were measured in order to get the absorbed pump power P_{abs}. When the sample temperature was stabilized at ΔT above the room temperature, the pump beam was suddenly stopped, and the sample temperature decreased exponentially with a time constant τ determined from the experimental data.

The fractional thermal loading η (ratio of absorbed pump power converted to heat) is then obtained from the expression[16,17]

$$\eta = \frac{C_{\mathrm{p}} m \Delta T}{\tau P_{\mathrm{abs}}} \tag{3}$$

where $_{\mathrm{Cp}}$ is the heat capacity per unit mass and ΔT is the difference between the sample temperature and room temperature.

From spectroscopy, the fractional thermal loading was estimated as

$$\eta_{\mathrm{h}} = \frac{Q_1 + Q_2 + Q_3}{\frac{1}{\lambda_{\mathrm{p}}}} \tag{4}$$

where λ_{p} is the pump wavelength for the $^4F_{5/2}$ level, and $Q_1 = (1/\lambda_p) - (1/\lambda_E)$ is the heat due to the $^4F_{5/2} \rightarrow {}^4F_{3/2}$ nonradiative de-excitation (λ_E = absorption wavelength of the $^4F_{3/2}$ emitting level). $Q_2 = \eta_{NR}/\lambda_E$ is the heat due to the nonradiative de-excitation of the $^4F_{3/2}$ level with a quantum yield $\eta_{\mathrm{NR}} = 1 - \tau/\tau_0$, where τ_0 is the $^4F_{3/2}$ lifetime at weak Nd concentration and $\tau = \int_0^\infty (I(t)/I(0))\, dt$ is the effective fluorescence lifetime measured for a sample witht 1 atom % Nd concentration of the measured sample, taking into account that the decay is not exponential due to well-known cross-relaxation mechanisms.

$Q_3 = (1 - \eta_{\mathrm{NR}})((1/\lambda_E) - (1/\lambda_{\mathrm{eff}}))$ is the deposited heat following all the three radiative de-excitations at λ_1, λ_2, and λ_3 wavelengths from the $^4F_{3/2}$ emitting level at the effective λ_{eff} wavelength calculated including the measured branching ratios.

dx.doi.org/10.1021/jp5027493 | J. Phys. Chem. C 2014, 118, 13781−13789

We also obtained the thermal conductivity, κ, from the temperature distribution on the exit face of the sample measured with the Pyroview 380L thermal camera (image resolution: 46 μm/pixel). The 1 atom % Nd-doped YS1AG ceramics sample (6 × 6 mm^2 square, thickness: 2.5 mm) was pumped through its entrance face and cooled down from the four edges in close contact with a water cooled copper mount. The pump was the focused beam from the fiber coupled laser diode.

Modeling the heat process as axisymmetric around the z-axis, the temperature distribution inside the sample follows the well-known heat equation:

$$\frac{1}{r}\frac{\partial}{\partial r}\left(r\frac{\partial T}{\partial r}\right)+\frac{\partial^2 T}{\partial z^2}=-\frac{Q(r,z)}{\kappa} \tag{5}$$

where $Q(r, z)$ is the heat per unit volume deposited inside the sample by the pump, r is the radial coordinate, and z is the axial coordinate. We calculated the heat deposited with the expression

$$Q(r,z)=\eta_h\frac{(1-R)P_0}{\frac{\pi w_p^2}{2}}\alpha(e^{-\alpha z}+\mathrm{Re}^{-\alpha(l-z))})e^{-2r^2/w_p^2} \tag{6}$$

where α is the absorption coefficient, w_p is the average pump waist, l is the sample thickness, R is the face reflectivity, P_0 is the pump power, and η_h is the fractional thermal loading.

The Neumann conditions used for solving the heat equation are $\partial T/\partial z = 0$ at the entrance and exit faces, meaning that the heat exchange with air is neglected, $-\kappa(\partial T/\partial r) = H(T_{edge} - T_{Cu})$, at the edges of the sample in contact with the Cu mount. H is the heat transfer coefficient adjusted to reproduce the sample edge and Cu-mount measured temperatures.

Optical Parameter Determination. Optical transmittance was measured using a Cary 5000 spectrophotometer, with a double beam option. The samples were polished to optical grade quality. The thickness of the sample used in the measurements was 710 μm. The thermal dependence of the refractive index of YS1AG doped with neodymium was analyzed using a prism-film coupler system (Metricon model 2010), which scans the incident angle to determine the critical angle for total internal reflection (TIR). The refractive indices were measured at λ = 632.8 nm from room temperature to 415 K, which covers the range of temperature that suffers the crystal during laser operation.

For the nonlinear refractive index evaluation, the laser source used was a Ti Sapphire Oscillator (Tsunami, Spectra Physics) and a regenerative amplifier system (Spitfire, Spectra Physics) based on chirped pulsed amplification (CPA) operating at 795 nm with 120 fs pulses, a repetition rate of 1 kHz, and a bandwidth of 10 nm. The maximum pulse energy delivered by this system was 1 mJ, but it was reduced to the μJ level by using a calibrated neutral density filter, a $\lambda/2$ plate, and a polarizer. The beam was focused by a f = 200 mm lens in the sample, which was placed on a motorized stage to perform the scan of the sample along the propagation direction (z-axis) with 1 mm steps. In order to increase the effective Rayleigh range of the focused beam, a circular iris (diameter 4 mm) was placed before the lens. A beam splitter behind the focus of the lens allowed monitoring of the absorption of the sample in the near field by a charge-coupled device (CCD) camera (operating in integration mode). In the far field (more than 60 cm behind the focus), an iris limited the beam and a second CCD camera registered the transmitted signal. To determine the nonlinear refractive index, we used the expression[18,19]

$$n_2=\sqrt{2}\frac{\Delta T_{pv}}{0.406(1-S)^{0.25}I_0 L}\frac{\lambda}{2\pi} \tag{7}$$

where ΔT_{pv} is the change in the transmittance from the valley to the peak, I_o is the peak intensity at the focus of the lens, L is the thickness of the sample, λ is the wavelength of the beam used for the experiments, n_2 is the nonlinear refractive index, and S is the transmittance of the iris.

3. RESULTS AND DISCUSSION

3.1. Structure and Microstructure of YS1AG and Nd:YS1AG Ceramics. Table 1 summarizes the chemical composition of the studied samples. It can be pointed out that the aluminum contents in the samples are lower than those corresponding to the theoretical stoichiometry. This could be related with the light nature of this element, which can be lost, partially, in the high-temperature sintering process. This lack of aluminum is compensated with an excess of Y(+Nd) and Sc. The neodymium contents agree with the expected neodymium concentration.

Table 1. Description of the Stoichiometry and Unit Cell Parameters of the YS1AG Microceramic Samples in This Work (MW Molecular Weight)

material	stoichiometry	MW	unit cell parameter [Å]
$Y_3ScAl_4O_{12}$	$Y_{3.03}Nd_{0.00}Al_{3.90}Sc_{1.07}O_{12}$	614.73	12.1757(3)
1% Nd:$Y_3ScAl_4O_{12}$	$Y_{3.00}Nd_{0.03}Al_{3.92}Sc_{1.05}O_{12}$	616.03	12.1738(7)
2% Nd:$Y_3ScAl_4O_{12}$	$Y_{2.98}Nd_{0.06}Al_{3.93}Sc_{1.03}O_{12}$	617.95	12.1749(3)

Figure 2 shows the obtained XRD patterns for the YS1AG and Nd:YS1AG ceramics. We measured the crystallographic parameter (cubic system, space group $Ia{-}3d$ (N.230)) reported also in Table 1. These values are smaller than those previously reported in literature for YS2AG ($Y_3Sc_2Al_3O_{12}$) single crystal (Allik et al.[20] a = 12.271 Å; Kokta et al.[21] a = 12.324 Å, and Bogomalov et al.[22] a = 12.251 Å), which agrees with the lower content of Sc^{3+} in our ceramics, which has a larger ionic radius than Al^{3+}.

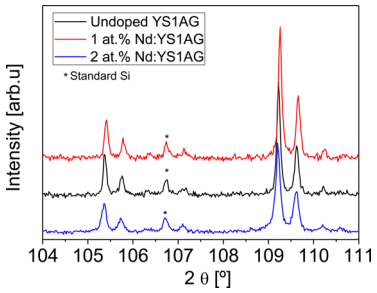

Figure 2. XRD patterns recorded for the Nd:YS1AG microceramics.

From the point of view of their occupation in $Y_3ScAl_4O_{12}$, Sc^{3+} and Al^{3+} are distributed stochastically at the same site, at the octahedral position, ScO_6 or AlO_6 (Wyckoff 16a) in garnet structure (ionic radii of these ions: Al^{3+} (VI) = 0.535 Å, Sc^{3+} (VI) = 0.745 Å[23]). Thus, this material has a disordered structure. Figure 3 shows the expected location of Sc^{3+} ions in the garnet structure. This figure is plotted using the atomic

dx.doi.org/10.1021/jp5027493 | J. Phys. Chem. C 2014, 118, 13781−13789

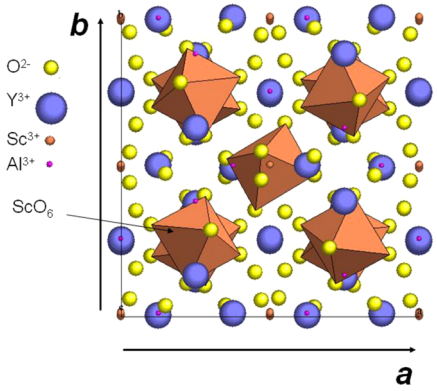

Figure 3. Projection of the YS2AG crystalline structure parallel to the [001] direction.

positions in a typical garnet structure, and assuming that all the Sc^{3+} ions substitute Al^{3+} ions in the octahedral position, as in the YS2AG compound. In YS1AG, Sc^{3+} is replacing Al^{3+} in the octahedral position with a ratio of 1/2. Y^{3+} is surrounded by eight O forming a YO_8 polyhedra (dodecahedral site, Wyckoff 24c), and the Nd^{3+} is expected to be substituted in this site due to the similarity of ionic radii (ionic radii, Y^{3+} (VIII) = 1.09 Å and Nd^{3+} (VIII) = 1.109 Å[24]). Finally, using the determined unit cell parameter from XRD analysis, the calculated molecular weight extracted from the chemical composition, and $Z = 8$, it is also possible to calculate the density of the ceramic samples reported in Table 2.

Figure 4 shows the microstructure of the 2 atom % Nd:YS1AG ceramic sample. From SEM observations (Figure 4a), the grain size appears to be rather homogeneous and close to 0.65 μm in size, whereas no visible secondary phases or residual porosity (relative density close to 100%) have been detected. The transmission electron microscopy (TEM) micrograph (Figure 4b) shows a triple point (i.e., junction between three grains) with no local segregation or other visible defects. To study the crystallinity of the observed nanocrystals, FFT patterns of the three regions of the HRTEM image were obtained (see insets in Figure 4b), which indicates the (hkl) reflections in the crystalline lattice. As can be observed in the figure, the grain with the highest level of crystallinity is in region number one.

3.2. Thermal Characterization. *3.2.1. Specific Heat.* The C_p measurements of undoped and Nd doped YS1AG samples were made in the range from 300 to 500 K, and the values obtained are shown in Figure 5. The values obtained at room temperature are in the range 0.81–0.90 J $g^{-1}K^{-1}$ (summarized in Table 2), being larger than that reported for undoped crystalline YAG (0.60 J $g^{-1}K^{-1}$). Assuming as a first approximation that the heat capacity of a polyatomic solid is the sum of the heat capacity of the constituent atoms; this increase in the specific heat in relation with YAG should be expected due to the substitution of Al^{3+} by heavier atom Sc^{3+}, which also has a larger atomic heat capacity. Additionally, the dependence of the specific heat with temperature and its value shows the typical behavior of a dielectric crystal.

3.2.2. Thermal Diffusivity. The thermal diffusivity is the parameter that determines the rate at which the thermal equilibrium is reached, and it depends linearly on the mean free path of the phonons and their speed. As it is mentioned in the Introduction, the thermal phonons are not affected by the boundaries in the ceramics, so the expected values of thermal diffusivity must be similar in bulk crystals and bulk ceramics. At high temperatures (higher than the Debye temperature) the mean free path of the phonons is proportional to 1/T, so the thermal diffusivity decreases with the increase of temperature. Figure 6 shows the variation of the thermal diffusivity with the temperature for undoped and Nd:YS1AG ceramic samples for two different concentrations of Nd doping.

The thermal diffusivities at 300 K are 2.40, 2.39, and 2.35 mm^2s^{-1} for the undoped, 1 atom % Nd-doped, and 2 atom % Nd-doped samples, respectively. The thermal diffusivity value tends to decrease with the increase of the Nd content; nevertheless, this slight variation is in the range of the precision of the technique of measurement. In comparison with other garnet structures, a larger value of 4.1 mm^2 s^{-1} at 300 K has been reported for crystalline YAG;[24] however, a smaller value of 1.94 mm^2 s^{-1} has been reported for GS2AG ($Gd_3Sc_2Al_3O_{12}$).[25] Then, the thermal diffusivity measured for the YS1AG ceramics in the present paper is in the expected range of values for a garnet material.

3.2.3. Thermal Conductivity. The thermal conductivity can be calculated by $\kappa = \rho \cdot D \cdot C_p$.[26] Thus, by using the density, the thermal diffusivity, and the specific heat, we can calculate the thermal conductivity dependence with temperature (assuming a constant density), as shown in Figure 7. The behavior observed is typical of a dielectric crystal in the temperature range studied, despite the structural disorder. For example, for the undoped sample, the thermal conductivity reaches a 70% of its value at room temperature, when we increase the temperature up to 500 K.[27] Table 2 summarizes the thermal conductivity values of YS1AG and Nd:YS1AG at room temperature. The thermal conductivity at room temperature is around 8.6–9.7 W m^{-1} K^{-1}, which is a rather competitive value compared to that of YAG crystal.

3.2.4. Fractional Thermal Loading. A $Y_{3.00}Nd_{0.03}Al_{3.92}Sc_{1.05}O_{12}$ sample was pumped with a 423 mW laser emitting at λ_p = 807 nm. The weight of the sample was 0.418 g, and it was observed that, due to energy absorption, its temperature increased up to 48 K above room temperature. After stopping the pump, the sample temperature decreased with a time evolution following an exponential evolution. The

Table 2. Thermal Properties, Molecular Weight, and Density of Garnet Structures and Nd:YS1AG Microceramics

material	MW[a]	C_p [J $g^{-1}K^{-1}$]	ρ [g cm^{-3}]	D [mm^2s^{-1}]	κ [W $m^{-1}K^{-1}$]	ref
$Y_3Al_5O_{12}$ (crys)[b]	593.616	0.59	4.56	4.1	11.22	24
$Gd_3Sc_2Al_3O_{12}$(crys)	861.59	0.43	5.71	1.94	4.76	25
$Y_3ScAl_4O_{12}$ (cer)[c]	614.73	0.83	4.524	2.40	9.06	this work
1% Nd: $Y_3ScAl_4O_{12}$(cer)	616.03	0.90	4.535	2.39	9.71	this work
2% Nd:$Y_3ScAl_4O_{12}$(cer)	617.95	0.81	4.548	2.35	8.66	this work

[a]MW: molecular weight. [b]crys: single crystal. [c]cer: ceramics.

dx.doi.org/10.1021/jp5027493 | J. Phys. Chem. C 2014, 118, 13781–13789

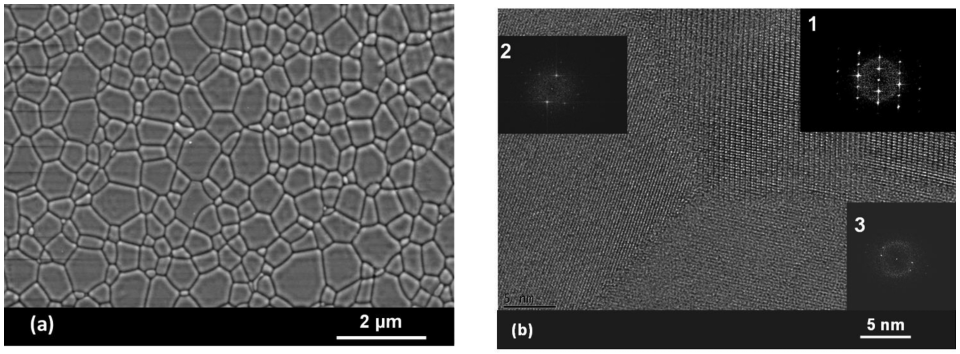

Figure 4. SEM (a) and TEM (b) micrographs corresponding to the 2 atom % Nd:YS1AG microceramics obtained after vacuum sintering at 2023 K for 10 h. Insets: FFT patterns of the different ceramic grains.

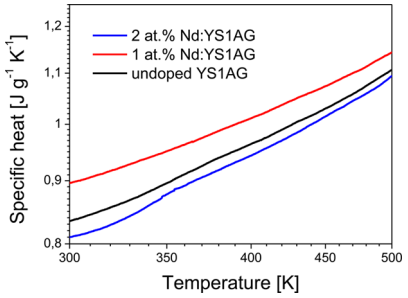

Figure 5. Temperature evolution of the specific heat (C_p) corresponding to the YS1AG and Nd:YS1AG microceramics.

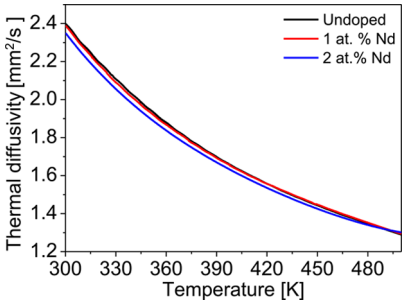

Figure 6. Temperature evolution of the thermal diffusivity of the YS1AG and Nd:YS1AG ceramic samples.

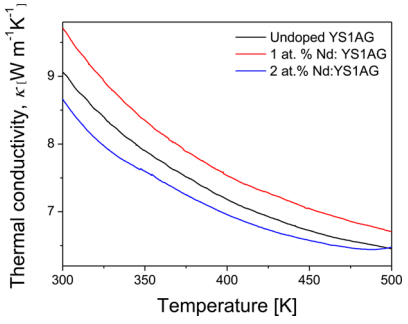

Figure 7. Temperature evolution of the thermal conductivity, κ, of the YS1AG and Nd:YS1AG microceramics.

time constant was 75.3 s, leading to a fractional thermal loading of 49%.

From our spectroscopic measurements, the involved wavelengths are λ_E = 880 nm and 902.8, 1076.1, 1358.5 for the radiative transitions toward the $^4I_{9/2}$, $^4I_{11/2}$, and $^4I_{13/2}$ levels, with branching ratios 0.32, 0.57, and 0.11, respectively. So we obtained the wavelength λ_{eff} of the effective transition in Figure 1 as $1/\lambda_{eff} = 0.32/902.8 + 0.57/1076.1 + 0.11/1358.5$. From the decay time measurements we found τ = 188.4 μs, while we took τ_0 =280 μs from the literature.[6] The spectroscopic method led to an estimation of 47.5% fractional thermal loading, which is similar to that from the temperature evaluation method. A similar procedure led to 38% fractional thermal loading for a 0.8% Nd-doped YAG sample. The spectroscopic method was used to estimate the fractional thermal load of the 2% Nd-doped YS1AG sample, which resulted in a 55% fractional thermal loading, using a decay time of τ = 160 μs.

3.2.5. Thermal Conductivity Determined from Thermal Loading and Temperature Distribution. To study the temperature distribution in the sample, the radial, r, and axial, z, coordinates are commonly used in the literature. The (r,z)-dependence of the temperature was made explicit by Chen[28] and Innocenzi[29] with an analytical solving method that neglects the z-derivative in order to consider only the radial heat flow. This method was refined later.[30−32] However, the analytical solutions published up to now exhibit a temperature gradient along the z-axial direction of the form of $\exp(-\alpha z)$ (the same dependence than the absorbed pump) which was not validated by our method.[33] Our numerical solution of the heat equation using Matlab without neglecting any axial thermal transfer, shows that the axial temperature distribution calculated at the central axis (r = 0) of the sample is far to have an $\exp(-\alpha z)$ dependence (see curve (a) in Figure 8). This is the signature, together with the radial transfer, that some heat is transferred from the vicinity of the entrance face (which can be very hot due to axial nonuniform pump) toward the exit face (which is much less hot). This is because, in reality, the axial conductivity

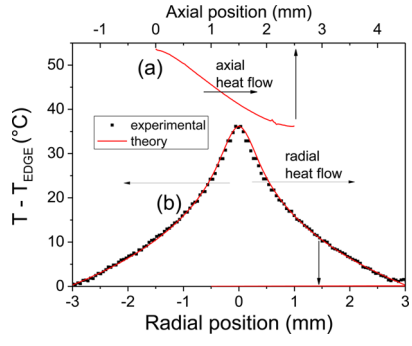

Figure 8. (a) Axial (r = 0) and (b) radial temperature distribution on the exit face (z = 2.5 mm) of the 1 atom % Nd:YS1AG ceramic.

dx.doi.org/10.1021/jp5027493 | J. Phys. Chem. C 2014, 118, 13781−13789

is not zero, to the contrary of the simplifying approximation used in eqs 1−5.

The experimental radial temperature distribution, obtained under an incident power of 5.85 W incident power at 808 nm, was well represented by our model (see curve (b) in Figure 8) with a fitting value for the thermal conductivity κ_c = 6.9 W $m^{-1}K^{-1}$ and the average value w_p = 340 μm. Because the edge temperature of the sample was close to 22 °C, the value of κ_c measured in this section involves a sample temperature in the 22−77 °C range (entrance face) and has to be understood as an average value. This value is lower than that at room temperature (close to 9.7 W m^{-1} K^{-1}), but it is in agreement with subsection 3.2.2 showing the decrease of the thermal conductivity with temperature. This average κ_c value has the interest to be measured in experimental conditions very close to those ones used in a diode end-pumped pumping laser cavity.

3.3. Optical Characterization. *3.3.1. Optical Transmittance.* The optical transmittance of the $Y_{3.00}Nd_{0.03}Al_{3.92}Sc_{1.05}O_{12}$ sample (thickness 710 μm) is shown in Figure 9, without reflectance correction. The cutoff of the optical transmittance in the UV−visible range was defined as the wavelength where the maximum transmission is decreased by a 1/*e* factor and is located at around 235 nm. The transmittance at 700 nm (where there is no neodymium absorption) is around 80% (according to the refractive index measured at 632 nm, the specular reflectivity should be around 9%). This high value of transmittance agrees with the low density of microstructural defects (pores, secondary phases) observed in the ceramic samples.

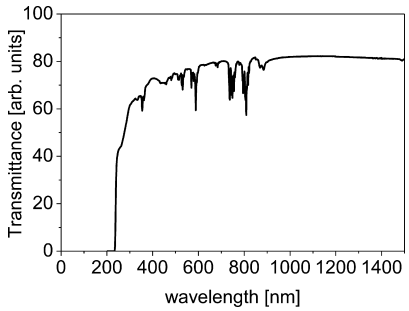

Figure 9. Optical transmittance of the 1 atom % Nd:YS1AG ceramic sample with a thickness of 710 μm.

3.3.2. Linear Refractive Index and Thermo-optic Coefficient. The refractive index and its dependence with temperature are related to the polarizability and density of the material. In fact, the temperature dependence of the density is related to the volumetric expansion coefficient of the crystallographic unit cell. Usually, the density, and hence the refractive index, decrease with temperature owing to the positive volumetric expansion coefficient of the crystallographic unit cell, which leads to a negative thermo-optic coefficient. Furthermore, a positive change in polarizability with temperature (an increase of the thermal occupancy of the energy levels of the material as a function of temperature) leads to a lower fundamental phonon frequency, ω_0, and an optical band gap, E_g, which, in ionic crystals, results in an increase of the refractive index, i.e., a positive thermo-optic coefficient.[34] As it can be observed in Table 3, the YS1AG ceramic materials possess a positive thermo-optic coefficient, as other garnet structures. This means that the polarizability of the material plays a more important role that the thermo-optic coefficient. The values measured for the different samples are in the same range 12.8−13.3 × 10^{-6} K^{-1}.

Figure 10 shows the evolution of the refractive index with temperature for the undoped and Nd doped samples. As can be seen in this figure, the refractive index of Nd:YS1AG decreases as the Nd concentration increases.

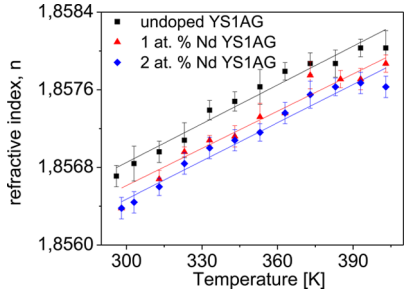

Figure 10. Temperature evolution of the linear refractive index for the YS1AG and Nd:YS1AG microceramics.

3.3.3. Nonlinear Refractive Index, n_2. The measurement of n_2 for the undoped YS1AG sample was performed at several peak intensities, as is shown in Figure 11. The signal obtained

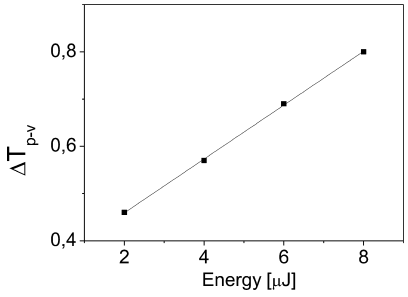

Figure 11. Dependence of the transmittance difference valley peak with the energy of the pulse for undoped YS1AG microceramics.

Table 3. Optical Properties of Garnet Structures and Nd:YS1AG Microceramics

material	n (λ,nm)	MW	dn/dt [10^{-6} K^{-1}] (λ,nm)	n_2 [10^{-13} esu] (λ,nm)	ref
$Y_3Al_5O_{12}$ (crys)	1.8295(632)	593.616	9.3 (633)	2.7(1060)	35
$Y_3Al_5O_{12}$(crys)	-		15 (632)	-	36
$Gd_3Sc_2Al_3O_{12}$(crys)	1.9640(632)	861.59	5.48 (632)	5.5(1060)	37
Nd:$Y_3Sc_2Al_2GaO_{12}$ (crys)	-	-	44	-	38
$Y_3ScAl_4O_{12}$ (cer)	1.8567(632)	614.73	13.3(632)	2.5 (795)	this work
1% Nd:$Y_3ScAl_4O_{12}$(cer)	1.8564(632)	616.03	12.8(632)	-	this work
2% Nd:$Y_3ScAl_4O_{12}$(cer)	1.8564(632)	617.95	13.2(632)	-	this work

dx.doi.org/10.1021/jp5027493 | J. Phys. Chem. C 2014, 118, 13781−13789

was not homogeneous, and we also observed a discrepancy on the signal depending of the incidence point on the sample, indicating a certain degree of inhomogeneity in the ceramic sample.

Nevertheless, using the experimental transmittance valley−peak difference, the n_2 calculated is 5.5×10^{-16} cm^2W^{-1} (2.5×10^{-13} esu). Usually materials belonging to the garnet family present n_2 values higher than 2.5×10^{-13} esu, being the lowest one for YAG. Additionally, n_2 shows a linear dependence with the linear refractive index and with the polarizability of the constituent anions: since YS1AG ceramic has a larger linear refractive index than YAG (1.8567 versus 1.8295 at 632 nm) and also the Sc^{3+} shows higher polarizability than Al^{3+}, we believe that the n_2 value extracted from the experimental transmittance valley−peak difference of 2.5×10^{-13} esu is quite reliable.

4. CONCLUSIONS

High crystalline quality neodymium-doped YS1AG ceramics have been obtained by sintering at high temperatures. All the microceramics prepared belong to the cubic system with space group $Ia\bar{3}d$ and a unit cell parameter around 12.17 Å. The stoichiometry of all the samples shows that neodymium concentration corresponds to that introduced initially, and almost all have a slight deficiency of Al. The grain sizes of the ceramics are homogeneous, and no visible secondary phases or residual porosity was detected, accordingly to the high optical transmittance in the visible and near-infrared range measured. The dependence of the thermal conductivity with temperature shows the typical behavior of a dielectric crystal, despite the disorder present in the structure, with a value at room temperature around 9 W m^{-1} K^{-1}. The thermal properties of these ceramics are rather competitive, and the values obtained are similar to those of garnet crystals. The refractive index of these compounds at 632 nm measured at room temperature, are in the range 1.8564−1.8567, and the thermo-optic coefficient is positive, with values ranging from 12.8 to 13.3 $\times 10^{-6}$ K^{-1}. Finally, the n_2 value at 795 nm extracted from the experimental transmittance valley−peak is 2.5×10^{-13} esu, which is in agreement with the n_2 values for the garnet family of compounds. Summarizing, these ceramics are a promising alternative to the high-power laser host materials used at present.

AUTHOR INFORMATION

Corresponding Author

*Mailing address: Física i Cristal·lografia de Materials i nanomaterials (FiCMA-FiCNA)-EMAS, Universitat Rovira i Virgili, Campus Sescelades. c/Marcel·lí Domingo, s/n, 43007 Tarragona, Spain. Telephone number: 0034 977 55 86 28; e-mail: mariacinta.pujol@urv.cat.

Notes

The authors declare no competing financial interest.

ACKNOWLEDGMENTS

This work is supported by the Spanish Government under projects MAT2011-29255-C02-01-02, MAT2013-47395-C4-4-R, and the Catalan Government under project 2014SGR1358. It was also funded by the European Commission under the Seventh Framework Programme, project Cleanspace, FP7-SPACE-2010-1-GA No. 263044.

REFERENCES

(1) Merkle, L. D.; Dubinskii, M.; Schepler, K. L.; Hedge, S. M. Concentration Quenching in Fine-Grained Ceramic Nd:YAG. *Opt. Express* **2006**, *14*, 3893−3905.
(2) Ober, M. H.; Sorokin, E.; Sorokina, I.; Krausz, F.; Wintner, W.; Shcherbakov, I. A. Subpicosecond Mode-Locking of a Nd^{3+}-Doped Garnet Laser. *Opt. Lett.* **1992**, *17*, 1364−1366.
(3) Carreaud, J.; Labruyère, A.; Jaffres, L.; Couderc, V.; Maître, A.; Boulesteix, R.; Brenier, A.; Boulon, G.; Guyot, Y.; Rabinovitch, Y.; et al. Wavelength Switching in Nd:YSAG Ceramic Laser Induced by Thermal Effect. *Laser Phys. Lett.* **2012**, *9*, 344−349.
(4) Jaffres, L.; Labruyère, A.; Couderc, V.; Carreaud, J.; Maître, A.; Boulesteix, R.; Brenier, A.; Boulon, G.; Guyot, Y.; Rabinovitch, Y.; et al. Gain Structuration in Dual-Wavelength Nd:YSAG Ceramic Lasers. *Opt. Express* **2012**, *20*, 25596−25602.
(5) Ikesue, A.; Aung, Y. L.; Taira, T.; Kamimura, T.; Yoshida, K.; Messing, G. L. Progress in Ceramic Lasers. *Annu. Rev. Mater. Res.* **2006**, *36*, 397−429.
(6) Sato, Y.; Saikawa, J.; Taira, T.; Ikesue, A. Characteristics of Nd^{3+}-Doped $Y_3ScAl_4O_{12}$ Ceramic Laser. *Opt. Mater.* **2007**, *29*, 1277−1282.
(7) Bisson, J. F.; Yagi, H.; Yanagitani, T.; Kaminskii, A.; Barabanenkov, Y. N.; Ueda, K. I. Influence of the Grain Boundaries on the Heat Transfer in Laser Ceramics. *Opt. Rev.* **2007**, *14*, 1−13.
(8) Senatsky, Y.; Shirakawa, A.; Sato, Y.; Hagiwara, J.; Lu, J.; Ueda, K.; Yagi, H.; Yanagitani, T. Nonlinear refractive index of ceramic laser media and perspectives of their usage in a high-power laser-driver Laser. *Phys. Lett.* **2004**, *1*, 500−506.
(9) Carreaud, J.; Boulesteix, R.; Maître, A.; Rabinovitch, Y.; Brenier, A.; Labruyère, A.; Couderc, V. From Elaboration to Laser Properties of Transparent Polycrystalline Nd-Doped $Y_3Al_5O_{12}$ and $Y_3ScAl_4O_{12}$ Ceramics. A Comparative Study. *Opt. Mater.* **2013**, *35*, 704−711.
(10) Cheary, R. W.; Coelho, A. A. A Fundamental Parameters Approach to X-ray Line-Profile Fitting. *J. Appl. Crystallogr.* **1992**, *25*, 109−121.
(11) *TOPAS, General Profile and Structure Analysis Software for Powder Diffraction Data*, version 4.2; Bruker AXS GmbH: Karlsruhe, Germany, 2009.
(12) Chirtoc, M.; Dadarlat, D.; Bicanic, D.; Antoniow, J. S.; Egée, M. *Progress in Photothermal and Photoacoustic Science and Technology*; Mandelis, A., Hess, P., Eds.; SPIE Optical Engineering Press: Bellingham, WA, 1997; Vol. 3.
(13) Delenclos, S.; Chirtoc, M.; Sahraoui, A. H.; Kolinsky, C.; Buisine, J. M. Assessment of Calibration Procedures for Accurate Determination of Thermal Parameters of Liquids and Their Temperature Dependence Using the Photopyroelectric Method. *Rev. Sci. Instrum.* **2002**, *73*, 2773−2780.
(14) Salazar, A. On the Influence of the Coupling Fluid in Photopyroelectric Measurements. *Rev. Sci. Instrum.* **2003**, *74*, 825−827.
(15) Siegel, R.; Howell, J. R. *Thermal Radiation Heat Transfer*, 4th ed; Taylor and Francis Group: New York, 2001.
(16) Pinnow, D. A.; Rich, T. C. Development of a Calorimetric Method for Making Precision Optical-Absorption Measurements. *Appl. Opt.* **1973**, *12*, 984−992.
(17) Fan, T. I. Heat-Generation in Nd-YAG and Yb-YAG. *IEEE J. Quantum Electron.* **1993**, *29*, 1457−1459.
(18) Sheik-Bahae, M.; Said, A. A.; Wei, T. H.; Hagan, D. J.; Van Stryland, E. W. Sensitive Measurement of Optical Nonlinearities Using a Single Beam. *IEEE J. Quantum Electron.* **1990**, *26*, 760−769.
(19) Thilmann, N.; Strömqvist, G.; Pujol, M. C.; Pasiskevicius, V.; Petrov, V.; Diaz, F. Nonlinear Refractive Indices in Yb^{3+}-Doped and Undoped Monoclinic Double Tungstates $KRE(WO_4)_2$ where RE = Gd, Y, Yb, Lu. *Appl. Phys. B: Laser Opt.* **2009**, *96*, 385−392.
(20) Allik, T. H.; Morrison, C. A.; Gruber, J. B.; Kokta, M. R. Crystallography, Spectroscopic Analysis, and Lasing Properties of Nd^{3+}:$Y_3Sc_2Al_3O_{12}$. *Phys. Rev. B* **1990**, *41*, 21−30.
(21) Kokta, M. Solubility Enhancement of Nd^{3+} in Scandium Substituted Rare Earth-Aluminum Garnets. *J. Solid State Chem.* **1973**, *8*, 39−42.

(22) Bogomolova, G. A.; Bumagina, L. A.; Kaminskii, A. A.; Malkin, B. Z. Crystal Field in Laser Garnets with TR^{3+} Ions in the Exchange Charge Model. *Sov. Phys. Solid State* **1977**, *19*, 1428−1435.
(23) Shannon, R. D. Revised Effective Ionic Radii and Systematic Studies on Interatomic Distances in Halides and Chalcogenides. *Acta Crystallogr.* **1976**, *A32*, 751−767.
(24) Aggarwal, R. L.; Ripin, D. J.; Ochoa, J. R.; Fan, T. Y. Measurement of Thermo-Optic Properties of $Y_3Al_5O_{12}$, $Lu_3Al_5O_{12}$, $YAIO_3$,$LiYF_4$, $LiLuF_4$, BaY_2F_8, $KGd(WO_4)_2$, and $KY(WO_4)_2$ Laser Crystals in the 80−300 K Temperature Range. *J. Appl. Phys.* **2005**, *98*, 103514(14pp).
(25) Rand, D.; Miller, D.; Ripin, D. J.; Fan, T. Y. Cryogenic Yb^{3+}-Doped Materials for Pulsed Solid-State Laser Applications. *Opt. Mater. Express* **2011**, *1*, 434−450.
(26) Parker, W. J.; Jenkins, R. J.; Butler, C. P.; Abbott, G. L. Flash Method of Determining Thermal Diffusivity, Heat Capacity, and Thermal Conductivity. *J. Appl. Phys.* **1961**, *32*, 1679−1684.
(27) Sato, Y.; Taira, T. The Studies of Thermal Conductivity in $GdVO_4$, YVO_4, and $Y_3Al_5O_{12}$ Measured by Quasi-One Dimensional Flash Method. *Opt. Express* **2006**, *14*, 10528−10536.
(28) Chen, Y. F.; Huang, T. M.; Kao, C. F.; Wang, C. L.; Wang, S. C. Optimization in Scaling Fiber-Coupled Laser-Diode End-Pumped Lasers to Higher Power: Influence of Thermal Effect. *IEEE J. Quantum Electron.* **1977**, *33*, 1424−1429.
(29) Innocenzi, M. E.; Yura, H. T.; Fincher, C. L.; Field, R. A. Thermal Modeling of Continuous-Wave End-Pumped Solid State Lasers. *Appl. Phys. Lett.* **1990**, *56*, 1831−1833.
(30) Chenais, S.; Balembois, F.; Druon, F.; Lucas-Leclin, G.; Georges, P. Thermal Lensing in Diode-Pumped Ytterbium Lasers − Part I: Theoretical Analysis and Wavefront Measurements. *IEEE J. Quantum Electron.* **2004**, *40*, 1217−1234.
(31) Chenais, S.; Druon, F.; Forget, S.; Balembois, F.; Georges, P. On Thermal Effects in Solid-State Lasers: The Case of Ytterbium-Doped Materials. *Prog. Quantum Electron.* **2006**, *30*, 89−153.
(32) Didierjean, J.; Herault, E.; Balembois, F.; Georges, P. Thermal Conductivity Measurements of Laser Crystals by Infrared Thermography. Application to Nd: Doped Crystals. *Opt. Express* **2008**, *16*, 8995−9010.
(33) Brenier, A.; Alombert-Goget, G.; Guyot, Y.; Boulon, G. Laser and Thermal Properties of Nd:$YGd_2Sc_2Al_2GaO_{12}$. *Laser Phys. Lett.* **2012**, *9*, 697−703.
(34) Prod'homme, L. A New Approach to the Thermal Change in the Refractive Index of Glasses. *Phys. Chem. Glasses* **1960**, *1*, 119−122.
(35) Zharikov, Y. V.; Stodenikin, P. A.; Chikov, V. A.; Shigorin, V. D.; Privis, Y. S.; Shcherbakov, I. A. *Temperature Measurement of Refractive Indices of Rare-Earth Gallium Garnets*; General Physics Institute: Moscow, 1987; Report 190.
(36) Nunes, A. R.; Rohling, J. H.; Medina, A. N.; Pereire, J. R. D.; Bento, A. C.; Baeso, M. L.; Nunes, L. A. O.; Catunda, T. Time-Resolved Thermal Lens Determination of the Thermo-optical Coefficients in Nd-Doped Yttrium Aluminium Garnet as a Function of Temperature. *Appl. Phys. Lett.* **2004**, *84*, 5183−5185.
(37) Hoefer, C. S.; Kirby, K. W.; DeShazer, L. G. Thermo-optic Properties of Gadolinium Garnet Laser Crystals. *J. Opt. Soc. Am. B* **1988**, *5*, 2327−2332.
(38) Brenier, A.; Alombert-Goget, G.; Guyot, Y.; Boulon, G. Laser and Thermal Properties of Nd:$YGd_2Sc_2Al_2GaO_{12}$ Garnet Ceramic. *Laser Phys. Lett.* **2012**, *9*, 697−703.